Effects of photon and thermal coupling mechanisms on the characteristics of self-assembled InAs/GaAs quantum dot lasers

C. Y. Jin,* H. Y. Liu, K. M. Groom, Q. Jiang, and M. Hopkinson
Department of Electronic and Electrical Engineering, EPSRC National Center for III-V Technologies, University of Sheffield, Sheffield S1 3JD, United Kingdom

T. J. Badcock, R. J. Royce, and D. J. Mowbray
Department of Physics and Astronomy, University of Sheffield, Sheffield S3 7RH, United Kingdom
(Received 23 April 2007; published 9 August 2007)

The relative contributions of the photon and thermal coupling mechanisms to the behavior of self-assembled InAs/GaAs quantum dot lasers are studied. A theoretical model, which takes into account a photon coupling process between the ground and first excited states of different sized dots, is proposed to fully explain the temperature dependence of the threshold current density (J_{th}) of both undoped and *p*-doped lasers. The simulation results suggest that the carrier distribution between the different energy states in a dot is modulated by the intradot thermal excitation of carriers. This process, when combined with the photon coupling mechanism, can account for the negative characteristic temperature (T_0) appearing in different temperature ranges for undoped and *p*-doped devices. Thermal coupling, which involves thermal carrier escape and recapture among different dots, has also been studied. Below threshold, thermal coupling is found to be significant but is weakened as threshold is approached because of the decreased carrier lifetime. Near and above threshold, the photon coupling mechanism is important and can be used to model the different temperature behaviors of the lasing spectra observed experimentally for the undoped and *p*-doped lasers.

DOI: 10.1103/PhysRevB.76.085315 PACS number(s): 42.55.Px, 73.63.Kv

I. INTRODUCTION

In the early 1980s, a three-dimensional confinement structure, which was initially named a "quantum box", was theoretically proposed to eliminate the temperature dependence of the lasing threshold in semiconductor devices.[1,2] Since the 1990s, the use of strain-induced self-assembled quantum dots (QDs) has made it possible to form defect-free, three-dimensional confinement structures suitable for application in semiconductor lasers.[3] The first demonstration of a QD laser based on self-assembled QDs was reported by Kirstaedter *et al.* in 1994.[4] Following initial results, the performance of QD lasers was improved considerably, with a significantly lower threshold than for quantum well lasers achieved by many groups.[5–7] However, due to the existence of several nonideal factors, for example, finite-potential barriers,[5] excited QD states (ES),[8] and inhomogeneous broadening of the optical transitions,[9] the threshold current density (J_{th}) of present self-assembled QD lasers exhibits characteristic temperatures (T_0) departing significantly from the infinite value predicted for an ideal QD laser.[1]

A negative T_0 (a decreasing threshold current with increasing temperature) has been typically observed in undoped QD lasers at low temperatures ($\leqslant$200 K) and has been explained by a thermal coupling model (or thermal redistribution model) involving a transition from a nonequilibrium to an equilibrium carrier distribution within the QDs of the ensemble.[9,10] Evidence for this carrier thermal coupling process has been provided by photoluminescence (PL) spectra exhibiting two unusual behaviors with increasing temperature: (1) a spectral linewidth narrowing[11,12] and (2) a wavelength redshift in addition to the normal redshift arising from the band gap shrinkage.[13,14] Additional evidence for spectral linewidth narrowing has been obtained from the observation of thermal broadening phenomenon in laser emission spectra at low temperatures ($\leqslant$200 K).[15] By comparing the temperature-dependent threshold current and laser emission spectra of two QD lasers with different barrier heights, further evidence has been obtained supporting the thermal coupling model.[16] Theoretical analysis of this behavior has also been undertaken based on two major models: the master equation model[17,18] and the rate equation model.[19] However, although the thermal coupling model is able to successfully explain the negative T_0, the mechanism responsible for the low-temperature broadening of the laser emission spectra is still the subject of much debate. A possible problem with the thermal coupling model is whether interdot carrier transfer is sufficiently fast in comparison with the short carrier lifetime near threshold.[20,21] Moreover, the additional wavelength redshift phenomenon has only been observed in PL and has not yet been reported for laser emission spectra.

To improve the T_0 value at and above room temperature (RT) in 1.3 μm emitting QD lasers, *p*-type modulation doping has been incorporated with the aim of reducing the effects of hole excitation out of the lasing state.[22,23] A very high or even infinite T_0 has been demonstrated using this approach.[24–26] Further improvement of the room-temperature performance of 1.3 μm emitting QD lasers was reported recently[27,28] using a combination of *p*-type modulation doping and high-growth-temperature GaAs spacer layers placed between the QD layers.[29,30] In this and other work,[25] an infinite or negative T_0 has been reported, extending to temperatures as high as $\sim$50 °C.

While the reduction of hole excitation out of the lasing state should improve T_0, it cannot explain an infinite or negative value, and hence other possible mechanisms have been

considered. Experimental results from a measurement of the turn-on delay time and the unamplified spontaneous emission have been interpreted in terms of a decrease in both the nonradiative Auger and radiative recombination of the QDs, and this has been proposed as the process responsible for the infinite or negative T_0 around RT.[25,31] However, possible physical mechanisms for these effects are unclear. Alternatively, it has been proposed that the decrease of the threshold current density results from an interdot carrier thermal redistribution, which still occurs around RT in *p*-doped structures because the positive charged QDs, a result of the extrinsic holes, increase the confinement energy for electrons. Recently, a thermal redistribution delayed to ~270 K in a *p*-type QD laser has been observed by measuring the gain spectra at the transparency point[32] and by the behavior of low-injection current EL spectra.[33] These results have been interpreted as evidence for the translation of the thermal carrier redistribution induced negative T_0 region to higher temperature in *p*-type-doped devices. However, the thermal-carrier redistribution process is a one-way effect with increasing temperature (the thermal redistribution can only increase with increasing temperature) and hence cannot explain the observation of a positive T_0 in *p*-doped QD lasers at low temperature, a region where a negative T_0 exists in undoped QD lasers. In addition, our previous work suggested that a thermal-carrier redistribution process cannot solely explain the behavior of the temperature-dependent PL and the laser emission spectra.[28] To fully explain the different temperature behaviors of *p*-doped and undoped QD lasers, a photon coupling model has been developed.[28]

The purpose of this paper is to study the relative contributions of the thermal coupling mechanism (TCM) and the photon coupling mechanism (PCM) to the behavior of self-assembled QD lasers. A theoretical model which includes both the TCM and PCM is developed to explain the various experimental observations reported for QD lasers. The linewidth and emission wavelength of the temperature-dependent optical spectra, both below and above threshold, have been investigated experimentally and simulated using our model. Via a detailed comparison between *p*-doped and undoped devices, we find that although the TCM model can explain some of the experimental behavior, the PCM provides a better description of the full range of experimental data. Our main conclusion is that the TCM is dominant for subthreshold behavior, whereas the PCM makes a major contribution to both the threshold performance and lasing behavior.

The paper is organized as follows: We first describe the samples and the experimental details in Sec. II. In Sec. III, we present the theory developed to describe the temperature behavior of QD lasers. In Sec. IV, we discuss the relative contributions of the TCM and PCM. Finally, we summarize our conclusions in Sec. V.

II. EXPERIMENTAL DETAILS

Both *p*-type modulation doped and undoped QD laser structures were grown by molecular beam epitaxy in an Oxford Instruments V90H system. The *p*-type modulation doped device consists of five layers of InAs QDs, each grown within an 8 nm $In_{0.15}Ga_{0.85}As$ quantum well to give a dot-in-a-well (DWELL) structure.[5] Each DWELL is separated by 50 nm GaAs spacer layers. These dot and well parameters have been shown to optimize the optical properties of the InAs QDs.[34] In the GaAs spacer layer, 6 nm of GaAs is doped with Be at a level 1.0×10^{18} cm^{-3}, with the doped layer separated from the DWELL by 9 nm of undoped GaAs. This doping density results in approximately 15 acceptors per QD. An identical structure but with undoped spacer layers was grown for comparison. The growth temperature was 510 °C for the In-containing layers. Following the InAs QDs and the InGaAs well, the initial 15 nm of the GaAs spacer layer (SPL) was deposited at 510 °C, following which the temperature was increased to 580 °C for the remainder of the GaAs SPL. This low-to-high growth temperature step is critical for the growth of high quality structures without producing a shift in the wavelength from the required 1.3 μm.[29,35] The active region was grown at the center of an undoped 150 nm GaAs/AlGaAs waveguide with *n*-type lower and *p*-type upper cladding layers consisting of 1.5 μm $Al_{0.4}Ga_{0.6}As$ deposited at 620 °C. A heavily doped 300 nm p^+-GaAs contact layer completed the growth.

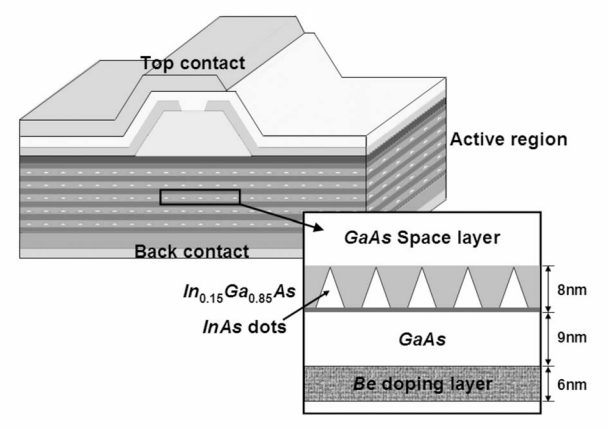

FIG. 1. A schematic diagram of the *p*-type modulation doped QD laser structure.

Shallow ridge waveguide lasers, as shown in Fig. 1, were fabricated by a $SiCl_4$ inductively coupled plasma technique, with etching below the *p*-doped AlGaAs cladding layer. Laser cavity lengths were 3 mm with as-cleaved facets. Laser characteristics were measured under pulsed injection (5 μs, 10 kHz) from 60 to 380 K. The heavily doped p^+ top layer was etched off in PL test structures as it is strongly absorbing at the emission wavelength of the QDs.

The temperature dependence of J_{th} for both the *p*-doped and undoped lasers is plotted in Fig. 2. The inset shows laser emission spectra recorded at RT for an injection current 1.1 times the threshold current. The peak wavelengths of the laser emission are 1289 and 1302 nm for the undoped and *p*-doped devices, respectively. For the undoped QD laser, the threshold current density decreases with increasing temperature between 130 and 220 K, resulting in a negative T_0.[10] Above ~220 K, J_{th} increases gradually with increasing temperature, with a more rapid increase occurring above 320 K.

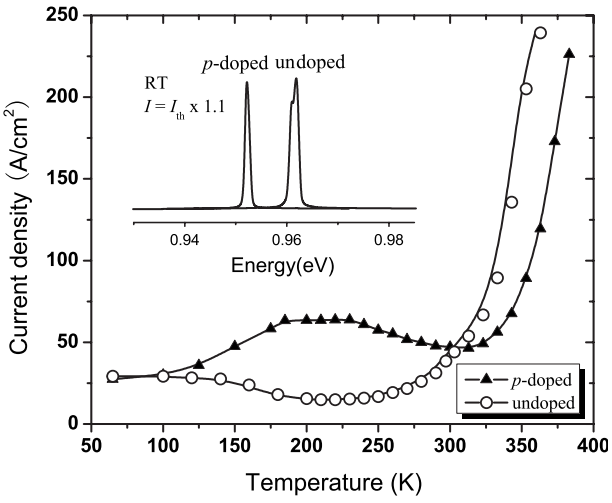

FIG. 2. Measured threshold current densities for both the *p*-doped and undoped lasers as a function of temperature. The inset shows laser emission spectra measured for a current $I=I_{\text{th}}\times 1.1$ at RT for both devices.

For the *p*-doped laser, the threshold current density initially increases gradually up to 200 K. Above 200 K, a negative T_0 occurs between 220 and 320 K (−50–50 °C). This is followed by an abrupt increase above 320 K. A threshold current density of 48 A cm^{-2} is achieved at RT for the *p*-doped structure.

III. THEORY

A. Thermal coupling mechanism and photon coupling mechanism

Figure 3 shows a schematic diagram of both the TCM and PCM in self-assembled QD lasers. In the thermal coupling process, carriers in smaller dots, which are assumed to have higher energy levels, are thermally excited into the barriers and are captured into larger dots which are generally those involved with the lasing. These additional carriers may increase the peak intensity of the optical spectra and hence the maximum gain for a given injection level. The concentration of carriers into one subset of QDs at high temperatures, compared to a uniform population at low temperatures, has been

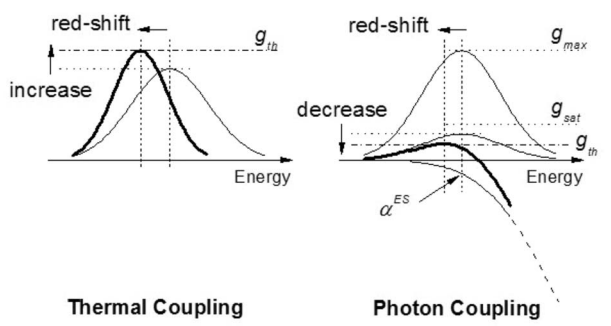

FIG. 3. Schematic diagrams of the thermal coupling mechanism (TCM) and photon coupling mechanism (PCM).

suggested as an explanation for the decrease of J_{th} in QD lasers as the temperature is increased.

Thermal coupling is a nonideal process resulting from the finite-potential barriers and the inhomogeneous broadening of the optical transitions. If the gain spectrum of a QD laser was dominated by the TCM, as shown in the left part of Fig. 3, three physical effects should be observed with increasing temperature and hence coupling: (1) a spectral linewidth narrowing, (2) a spectral intensity increase, and (3) a redshift of the emission maximum in addition to the normal redshift arising from band gap shrinkage. Thermal coupling is a monotonic process and can only increase with increasing temperature.

In the photon coupling process, we first assume that photons generated by the QDs can be either amplified or absorbed by transitions from both the ground state (GS) in similar sized dots and the excited state (ES) of larger dots; this process requires the presence of a distribution of QD sizes, which is unique to self-assembled quantum dot systems in that the optical properties comprise an inhomogeneous distribution of discrete states. Absorption or amplification occurs between GS and ES transitions, which are separated by less than the homogeneous broadening, $\hbar\Gamma_{h\nu}$.[36] Consequently, the total modal gain is the sum of the GS and ES gains at the relevant energy.

To re-emphasize the main physics of this model, the ES from larger dots which lie within the homogeneous broadening of the energy of the GS lasing transition contributes to the gain or loss at the lasing wavelength. This effect initially appears insufficient to affect the threshold current density. However, the GS gain usually saturates at about one-third of its possible maximum value around RT.[37] At any temperature, the threshold gain will be close to this value, while the ES gain can vary over a wide range, from almost the maximum ES absorption a_{max} to the threshold gain g_{th} as the thermal-carrier population of this state changes. Because the maximum ES absorption a_{max} is typically of order twice the maximum gain of the GS, the contribution from the ES transition at the lasing energy can be significant. As the energetic spacing of the hole levels is believed to be of the order of a few meV, compared to many tens of meV for the electrons, it is the thermal excitation of holes which is expected to make the major contribution to this process.[38] The right-hand side picture in Fig. 3 is plotted with parameters used in the following numerical simulations and with a maximum ES absorption at the lasing wavelength, α^{ES}. It is seen that with these parameters, a significant contribution from the ES occurs at the lasing wavelength.

The PCM is a nonideal process resulting from the existence of the ES levels and the inhomogeneous broadening of the discrete optical transitions. If the gain spectra of a QD laser were dominated by the PCM, as shown in the right hand side picture in Fig. 3, two effects should be observed with increased coupling, namely, (1) a spectral intensity decrease, which is due to the ES absorption at the lasing wavelength, and (2) a wavelength redshift, which is due to the asymmetry of the ES distribution around the lasing wavelength. For the PCM, either a coupling increase or decrease is possible with increasing temperature, reflecting either increased ES occupation by carrier excitation from the GS or

decreased ES occupation due to carrier escape to the barriers. When the coupling decrease in the PCM presents with increasing temperature, a spectral intensity increase and wavelength blueshift should occur.

Within both models, a negative T_0, indicating a decrease of J_{th}, should be reflected by an increase in the optical spectral intensity at the lasing wavelength. If we compare the main features of the TCM and PCM, a negative T_0 indicates a coupling increase in the TCM, which should be accompanied by a wavelength redshift. In contrast, a negative T_0 requires a coupling decrease within the PCM, and this should be accompanied by a wavelength blueshift. Therefore, from a study of the temperature-dependent peak wavelength of the laser emission, it should be possible to deduce the relative importance of the TCM and PCM.

An additional means by which the relative contributions of the TCM and PCM can be investigated is via their temperature dependence over a wide temperature range. The TCM is a monotonic process which can only result in an enhanced effect with increasing temperature. Therefore, this mechanism can only account for a negative T_0 and not a positive T_0. When using the TCM to explain the negative T_0 in both *p*-doped and undoped devices, a significant delay in the critical temperature for the onset of the thermal redistribution of carriers needs to be assumed for the *p*-doped devices. In addition, the TCM cannot explain the positive T_0 observed at low temperatures in *p*-doped devices (see Fig. 2). Such behavior requires the introduction of an entirely different process, for example, increased Auger recombination.[25] However, at present, this is an entirely phenomenal explanation,[32] with the physical mechanism responsible for an increasing Auger recombination unknown.

The PCM, however, can either be enhanced or reduced with increasing temperature. Hence, by appropriately applying this model, both the negative T_0 and the positive T_0 behaviors of a *p*-type modulation doped laser can be explained. In analysis the temperature behavior of the PCM, we introduce a second assumption that the thermal excitation of holes to higher QD energy levels occurs at lower temperatures than for electrons. This is a consequence of the more closely spaced hole levels. It is assumed that there are two critical temperatures, T_h and T_e, at which hole and electron thermal excitation to higher energy levels starts to occur. The second assumption requires that $T_h < T_e$.

For *p*-doped lasers, a large number of holes are released into the hole states of the QDs. Below T_h, the hole ES is fully occupied[39] and hence the ES absorption α^{ES} in Fig. 3 is blocked. Between T_h and T_e, the hole occupancy of the ES decreases due to thermal excitation to higher hole levels. As a result, state blocking of the ES absorption decreases and hence there is an increase in J_{th}, which causes a positive T_0 below T_e. Above T_e, due to the thermal excitation of electrons into the ES, absorption by the ES transition is increasingly blocked, resulting in a decreasing J_{th} and a negative T_0 value at RT. This decrease in J_{th} continues until carrier excitation to states in the barrier, followed by recombination in the barriers, and becomes significant, resulting in the observed abrupt increase in J_{th}. In contrast, for the undoped laser, below T_h, the electron and hole ESs are essentially unoccupied, so there is a strong ES absorption at the lasing wavelength. Above T_h, the ES absorption is gradually blocked by the thermal excitation of holes from the GS, resulting in a decrease of J_{th} (there is no parasitic recombination via the ES because there are no electrons in this state) and the observed negative T_0 at low temperatures. Above T_e, the ES absorption continues to be blocked, but recombination via the ES is now possible, resulting in a weakening of the decrease of J_{th}. Eventually, excitation to the barriers becomes significant and J_{th} starts to increase. Hence, the PCM is able to predict the occurrence of a negative T_0 over very different temperature ranges for undoped and *p*-doped QD lasers.

The PCM can also explain reports of a decrease in both the nonradiative Auger recombination[31] and radiative recombination[25] with increasing temperature via the predicted decrease of the GS occupancy. In addition, the increase of the nonradiative Auger recombination at low temperatures, which has been reported in some studies of *p*-doped lasers,[25] can be explained by the GS carrier density increase required to keep a constant g_{th} when the ES absorption increases in the *p*-doped device.

B. Rate equations

To theoretically investigate the relationship between the TCM and PCM, a theoretical model which can describe both the mechanisms has been developed. In Ref. 28, we described a rate equation model to study the PCM assuming an equal distribution of carriers within different QDs. In this work, we have further divided the QDs into subgroups. If we label different QD subgroups with $j=1,2,\ldots,J$, assuming an equal distribution of carriers within each QD subgroup, the rate equations for electrons can be written as follows:

$$\frac{\partial n_r}{\partial t} = \frac{I}{qV_a} - \sum_j \frac{V_{dots}^j}{V_a}(R_{cap}^j - R_{esc}^j) - \sum_{i=w,b}\left(\frac{V_i}{V_a}\frac{n_i}{\tau_i} + \frac{L}{V_a}\sum_\nu \Gamma_i g_i S\right), \tag{1}$$

$$\frac{\partial n_{ES}^j}{\partial t} = (R_{cap}^j - R_{esc}^j) - (R_{rel}^j - R_{ex}^j) - \frac{n_{ES}^j}{\tau_{ES}^j} - \frac{L}{V_{dots}^j}\sum_\nu \Gamma_{dots} g_{ES}^j S, \tag{2}$$

$$\frac{\partial n_{GS}^j}{\partial t} = (R_{rel}^j - R_{ex}^j) - \frac{n_{GS}^j}{\tau_{GS}^j} - \frac{L}{V_{dots}^j}\sum_\nu \Gamma_{dots} g_{GS}^j S, \tag{3}$$

where $n_r = \Sigma_{i=w,b}(V_i/V_a)n_i$ represents the normalized summation of electron densities in the well and barrier; n_{ES}^j and n_{GS}^j are the electron densities in the ground and excited states; I is the injected current, τ_b, τ_w, τ_{ES}^j, and τ_{GS}^j are the carrier lifetimes in the different regions; Γ_b, Γ_w, and Γ_{dots} are the optical confinement factors; g_b, g_w, g_{GS}^j, and g_{ES}^j are the material gains of the barriers, wells, and ground and excited states; V_a, V_b, V_w, V_{dots}^j are the volumes of the active region, barriers, wells, and the j_{th} subgroup of dots; L is the cavity length; and S represents the summation of the forward and backward propagating light densities: $(S^+ + S^-)$. $S^\pm$ obey the propagation rate equations:

$$\frac{\partial S^{\pm}}{v_g \partial t} \pm \frac{\partial S^{\pm}}{\partial z} = G_c S^{\pm} + R_{sp}, \tag{4}$$

where $G_c = \Sigma_j \Sigma_{i=b,w,GS,ES} \Gamma_i g_i^j - \alpha$ is the coupled optical modal gain, which describes the photon coupling process between the GS and first ES. We simply assume the same optical losses in different energy regions.

The second assumption of the PCM model is that the thermal excitation of holes to higher QD energy levels occurs at lower temperatures than that for electrons. In the numerical model, the hole distribution in the valence band is assumed to obey the Fermi-Dirac statistics above 80 K, whereas the electron distribution in the conduction band is determined by dynamical processes as described by the carrier rate equations (1)–(3). Charge neutrality is ensured by the following equation, which must be satisfied in each region of the device:

$$n = \sum_{i=w,b,dots} \left(\frac{V_i}{V_a} \right) n_i = p - p_A, \tag{5}$$

where V_i and n_i are the volume and electron densities for the barriers, wells, and dots, and p_A is the density of acceptors. We simply assume that all holes released from the Be impurities are captured into the dots, well, and barrier regions.

C. Gain and spontaneous emission

The modal gain of the QDs is described by[40]

$$g_i^j(\nu) = \frac{1}{h\upsilon} \frac{\chi_i}{V_0} \frac{\pi e^2 \hbar N_L}{c n_r \varepsilon_0 m_0^2} \int_{-\infty}^{\infty} |M_B|^2 |M_{cv}|^2 (f_i^{c,j} + f_i^{v,j} - 1) \times G_i^j(E') L_i(h\nu, E') dE', \quad i = GS, ES, \tag{6}$$

where $\chi_i = 2$ and 4 give the degeneracy of the ground and excited states, respectively, V_0 is the single dot volume, N_L is the dot layer number, n_r is the refractive index, M_{cv} is the wave function overlap, M_B is the Bloch matrix element, f^c and f^v are the occupation factors of the electron and hole, $G_i^j(E)$ is the Gaussian distribution function given by

$$G_i^j(E) = \frac{1}{\sqrt{2\pi}\sigma_i} \exp\left[-\frac{(E - E_i^j)^2}{2\sigma_i^2} \right], \quad i = GS, ES, \tag{7}$$

where σ_i is the width of the Gaussian distribution, and $L_i(h\nu, E)$ is the Lorentzian line shape given by

$$L_i(h\nu, E) = \frac{\hbar \Gamma_{cv,i}/\pi}{(E - h\nu)^2 + (\hbar \Gamma_{cv})^2}, \quad i = GS, ES, \tag{8}$$

where $\Gamma_{cv,i}$ is the carrier polarization dephasing rate.

The modal gains of the InGaAs wells and GaAs barriers are calculated as

$$g_i(\nu) = \Gamma_i a_i \rho_i (f_i^c + f_i^v - 1), \quad i = w, b, \tag{9}$$

where a_i is the gain coefficient and ρ_i is the reduce density of states.

The spontaneous emission coupled into different wavelengths in Eq. (4) can be defined as[41]

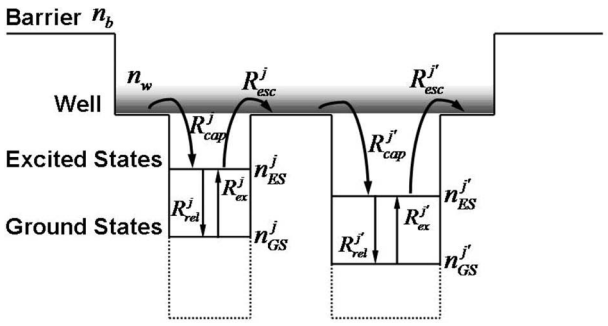

FIG. 4. A schematic diagram of electron transport processes in the conduction band of a quantum dot laser.

$$R_{sp}(\nu) = \sum_j \sum_{i=b,w,GS,ES} E_{st}^{i,j}(\upsilon) \Delta\nu, \tag{10}$$

where $\Delta\upsilon$ is the frequency separation between the cavity modes and E_{st} is the rate per unit length of stimulated emission, which can defined as follows:

$$E_{st}^{i,j}(\nu) = g_i^j(\nu) \frac{f_i^c f_i^v}{f_i^c + f_i^v - 1}, \quad i = w, b, GS, ES. \tag{11}$$

D. Carrier transfer process

Carrier transfer processes are defined in Fig. 4. The rate of carrier capture from the InGaAs wells into the dots is described by[42]

$$R_{cap}^j = \frac{n_w (1 - f_{ES}^{c,j})}{\tau_{cap}}, \tag{12}$$

where f_{ES} is defined as $f_{ES}^j = n_{ES}^j V_0 / \chi_{ES}$. The rate of carrier escape from the dots into the InGaAs wells is described by

$$R_{esc}^j = \frac{n_{ES}^j (1 - f_w^0)}{\tau_{esc}}, \tag{13}$$

where τ_{esc} is defined as $\tau_{esc} = \tau_{cap} \exp((E_w - E_{ES}^j)/kT)$,[43] with $E_w - E_{ES}^j$ denoting the energy difference between excited states and the InGaAs well band edge. The rate of carrier relaxation from the excited states to the ground state is given by

$$R_{rel}^j = \frac{n_{ES}^j (1 - f_{GS}^j)}{\tau_{rel}}, \tag{14}$$

where f_{GS}^j is defined as $f_{GS}^j = n_{GS}^j V_0 / \chi_{GS}$. The rate of carrier excitation from the ground state into the excited states is given by

$$R_{ex}^j = \frac{n_{GS}^j (1 - f_{ES}^j)}{\tau_{ex}}, \tag{15}$$

where τ_{ex} is defined as $\tau_{ex}=\tau_{rel}\exp((E^j_{ES}-E^j_{GS})/kT)$, with $E^j_{ES}-E^j_{GS}$ denoting the energy difference between the ground state and excited states.

E. Bimodal grouping of dot distributions and simulation results

An obvious method for grouping the dots is to divide them into subgroups based on their emission wavelength.[36] However, the main behavior difference, which can distinguish between the TCM and PCM, is an opposite wavelength shift of the emission in a negative T_0 temperature region. The wavelength shift is likely to be very small, about 10 nm over the full temperature range. To simulate the wavelength shift accurately using relatively small temperature steps, for example 20 K, a huge number of dot groups would need to be taken into account. This would be very computer intensive and so simplifications have to be found.

In this work, we divide the dots into two groups, each with a Gaussian distribution of energy levels. This implies $J=2$. These two groups reflect a bimodal distribution of QDs, which has been observed in many of our samples and in other reports.[35,44] Based on an atomic force microscopy analysis of our samples, we have assumed that a second distribution of QDs exists, which contains $\sim 10\%-30\%$ of the total number of QDs and represents QDs with a slightly smaller size. Although this bimodal grouping of the dot distribution may somewhat underestimate thermal effects within the same dot subgroup, it can successfully describe the continuous change of the spectral wavelength with increasing temperature while significantly saving on computational time.

The parameters used in the simulations presented in this paper are as follows. The dot density is $\rho_{dots}=4.3\times 10^{10}$ cm^{-2}, the height of the dots is $h_{dots}=6$ nm, and the width of the dots is $w_{dots}=15$ nm. The cavity length is $L=3$ mm, the width $W=10$ μm, and the thickness $d=0.4$ μm. The width of the $In_{0.15}Ga_{0.85}As$ well is $d_w=8$ nm, the width of the p-doped layer $d_p=6$ nm, and the distance between these two layers $d_{wp}=9$ nm. Optical confinement for the barriers is $\Gamma_b=0.06$, for the wells $\Gamma_w=0.01$, and for the dots $\Gamma_{dots}=0.0008$. The QD layer number is $N_L=5$. The facet reflectivity is $R_1=R_2=0.3$, optical loss $\alpha=2$ cm^{-1}, and refractive index $n_r=3.3$. The homogeneous broadening is assumed to have a Lorentzian form with $\hbar\Gamma_{cv}=6$ and 12 meV for the GS and ES, respectively. Within the models used, it is found that the lasing threshold is relatively insensitive to the homogeneous broadening. Hence a constant, temperature-insensitive homogeneous broadening is assumed, although experimentally, it has been shown that the homogeneous broadening does increase steadily over the temperature range considered in the simulations.[45,46] A Gaussian inhomogeneous broadening is assumed with values $\sigma_{GS}=16$ meV and $\sigma_{ES}=30$ meV for the GS and ES, respectively. The same broadening is used for both subsets of QDs. The density of acceptors for the p-doped device is $p_A=1.5\times 10^{18}$ cm^{-3}. We assume that all holes from the Be impurities are ionized into the barriers. The band gap of the GaAs barriers is $E^b_g=1.424$ eV, and the band gap of the $In_{0.15}Ga_{0.85}As$ well is 1.19 eV. In the simulation, only the electron ground state and the first excited state are included, whereas three hole levels are included. The separations of the electron and hole states are taken as 53 and 15 meV, respectively. The separation of the central energies of the two bimodal QD subsets is taken as 34 meV. It is assumed that 20% of the dots are in the second smaller size subset.

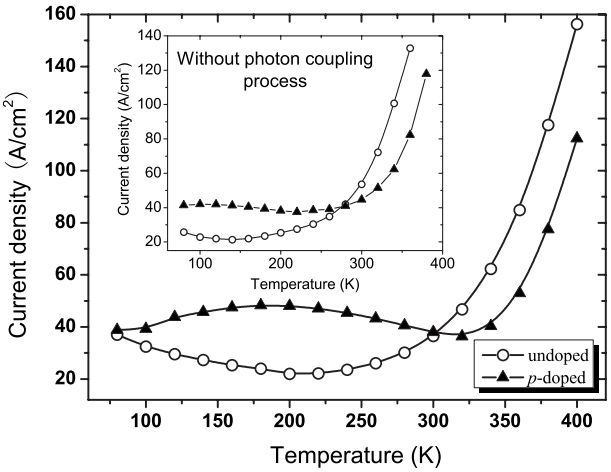

FIG. 5. Simulated temperature dependence of the threshold current densities for both the p-doped and undoped lasers. The inset shows the results of the simulation without the inclusion of the photon coupling process.

Figure 5 shows the results of the simulation of the temperature dependence of J_{th} for both the p-doped and undoped devices. These were obtained using the theoretical approach discussed above. A negative T_0 is predicted between 220 and 320 K for the p-doped laser. In addition, a negative T_0 is predicted for the undoped laser below 200 K. The results of the simulation show good agreement with the experimental results presented in Fig. 2. The inset of Fig. 5 shows the results of a simulation performed without the photon coupling process, obtained by simply ignoring the ES gain in the rate equation model. Only a very weak negative T_0 behavior is predicted in the temperature range from 140 to 220 K for the p-doped device, and 80–120 K for the undoped device. This negative T_0 results entirely from the TCM and is significantly weaker than the experimentally observed behavior. In addition, the low temperature positive T_0 behavior observed for the p-doped device is only reproduced when the PCM is included in the simulations.

The temperature dependence of the peak GS gain, normalized to the threshold gain, for an injection current $I=I_{th}\times 1.1$ is plotted in Fig. 6. The total optical gain, which is the sum of the GS gain and the ES gain at the lasing wavelength, equals the threshold gain at an injection level just above threshold. The normalized ES gain at the lasing wavelength will, therefore, be 1 minus the normalized peak gain of the GS (a small wavelength shift of the peak gain is neglected here). For the undoped device, the ES contribution at the lasing wavelength gives a strong absorption of $-0.26g_{th}$ at 80 K (hence the normalized GS gain has a value greater than 1), but with increasing temperature, it increases and eventually saturates to a positive value $\approx 0.16g_{th}$ above 200 K. For the p-doped device, the ES gain at the lasing wavelength is

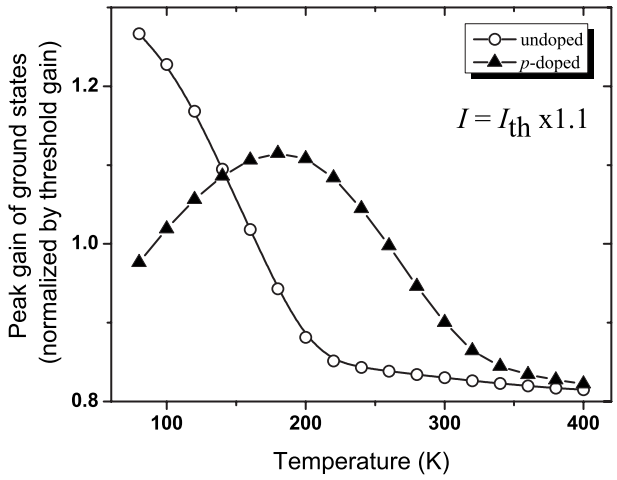

FIG. 6. Simulated maximum gain of the GS transition as a function of temperature. The gain is calculated for an injection current of $I_{\text{th}} \times 1.1$ and is normalized to the threshold gain.

zero at 80 K, corresponding to full Pauli blocking of the transition. With increasing temperature, the ES gain decreases to an absorption value of $-0.1 g_{\text{th}}$ at 200 K, followed by an increase and saturation to a positive value $\approx 0.16 \times g_{\text{th}}$ above 350 K. These calculations confirm the first assumption of the photon coupling model that the ES gain at the lasing wavelength can make a significant contribution to the total gain and can hence have a significant effect on the performance of the laser device.

The electron and hole occupancies of the ES for both devices are calculated as a function of temperature in Fig. 7(a) for an injection current $I = I_{\text{th}} \times 1.1$. For the p-doped laser, below 200 K, the hole occupation of the ES decreases due to intradot thermal excitation to higher confined states. This gives an increase in the ES absorption, as shown in Fig. 6, and hence a positive T_0. Above 200 K, the electron occupation of the ES increases due to intradot thermal excitation from the GS to the ES. This gives a decrease in the ES absorption and hence a negative T_0 near RT. In contrast, for the undoped laser, below 200 K, there is a strong increase in the electron occupation of the ES. As a result, a decrease of the ES absorption and a negative T_0 occur. The hole occupation level fluctuates very weakly in the undoped device because an equilibrium carrier distribution (Fermi-Dirac statistics) is assumed; this may slightly underestimate the holes' behavior at very low temperature ($\sim$100 K). Figure 7 reveals that, compared to the undoped device, the intradot thermal excitation of electrons into the ES is delayed in the p-doped device and this results in the negative T_0 appearing in a different temperature range for the two devices. In addition, the intradot thermal excitation of holes into the ES accounts for a positive T_0 appearing at very low temperatures in the p-doped device.

To investigate the reason why the excitation of electrons in the p-doped laser is delayed to higher temperatures, the electron and hole occupancies of the GS for both devices are plotted as a function of temperature in Fig. 7(b). When the carrier occupation factors for both holes and electrons are summed, a similar behavior to that exhibited by the gain, as

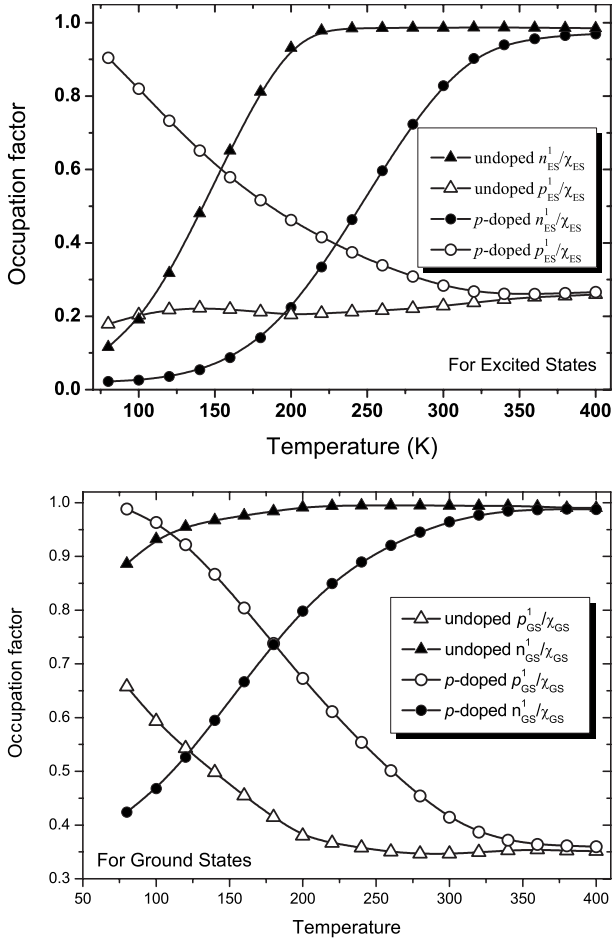

FIG. 7. Simulations of (a) the ES and (b) the GS carrier occupancies, for an injection current $I = I_{\text{th}} \times 1.1$, as a function of temperature for both the undoped and p-doped QD lasers.

shown in Fig. 6, is obtained. However, the electron occupation factor is lower in the p-doped device over the temperature range below 300 K. This is because the extrinsic holes in the QDs (see the hole occupation factor) result in fewer electrons being required to reach g_{th}. This reduced electron occupation decreases the excitation rate over the same temperature range because the intradot excitation of electrons is proportional to the electron density in the GS according to Eq. (15). Therefore, the onset for electron excitation out of the GS is shifted to higher temperatures. In addition the simulations show that the total GS occupation factor for both electrons and holes is approximately 1.35 for both devices over the temperature range studied. Referring to the expression for the gain in Eq. (6), the factor $(f^c + f^v - 1) \approx 0.35$ at threshold, which is near 1/3 of its maximum possible value (=1.0). Hence, the GS threshold gain is approximately 1/3 of the maximum gain, in agreement with the experimental report in Ref. 37. This finding also explains why the ES absorption is significant in the simulations shown in Fig. 6.

From Figs. 5–7, it can be seen that the value of T_h (the temperature where significant hole excitation out of the GS starts to occur) is less than 80 K for both the undoped and p-doped QD lasers; this is below the regime where the negative and positive T_0 behavior, start to occur for the undoped

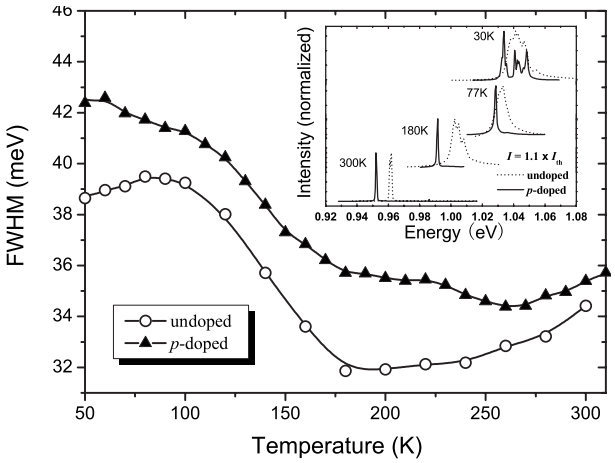

FIG. 8. PL FWHM for both the *p*-doped and undoped QD lasers as a function of temperature. The inset shows lasing spectra of the *p*-doped and undoped QD lasers for a number of different temperatures. The lasing spectra were recorded for a current $I(T)=I_{\mathrm{th}}(T)\times 1.1$.

and *p*-doped device, respectively (see Fig. 2). T_e has a value near 200 K for the *p*-doped device and is about 100 K for the undoped device, where the occupation factor exceeds a certain value (~0.2). These results indicate that the photon coupling process, modulated by the delay of the intradot excitation, is the main reason why the negative T_0 region appears at very different temperatures for the two devices. The results described in this section suggest that the PCM can be applied to explain the temperature dependence of J_{th} in both *p*-doped and undoped QD lasers.

IV. FURTHER RESULTS AND DISCUSSIONS

A theoretical model and numerical simulations have been applied to explain the very different temperature-dependent J_{th} behaviors of both undoped and *p*-doped QD lasers. Quantitative changes in the spectral intensity, which are responsible for the negative or positive T_0, have been analyzed. The PCM has been shown to provide a more complete description than the TCM in explaining the temperature dependence of J_{th} over the full experimental temperature range. However, two other processes, spectral linewidth narrowing and a wavelength redshift, both of which have been demonstrated as experimental support for the TCM,[11–14] have not yet been considered. In this section, these phenomena are studied, both below and above threshold, to further test the predictions of the TCM and PCM.

A. Spectral linewidth narrowing

The full width at half maximum (FWHM) of the PL spectra for the undoped and *p*-doped structures is plotted in Fig. 8 as a function of temperature. The FWHM of the *p*-doped structure is 2–4 meV larger than that of undoped structure, but the temperature range over which there is a rapidly decreasing FWHM is similar in both structures, from 100 to 180 K. Above this temperature range, the FWHM of the *p*-doped structure fluctuates near 35 meV, whereas the FWHM of the undoped structures slowly increases from 32 to 34.5 meV, between 180 and 300 K. Although the minimum of the PL linewidth is shifted to higher temperature in the *p*-doped device, the behavior is not fully consistent with the TCM. In particular, when compared to the temperature dependence of J_{th} in Fig. 2, the PL linewidth of the *p*-doped device reaches a minimum at a temperature (~260 K) below the temperature minimum of J_{th} (~310 K). In addition, at low temperatures between 100 and 180 K, although both devices exhibit a PL linewidth narrowing, their threshold current densities change in opposite directions. These experimental observations do not support a complete quantitative agreement between the TCM and temperature behavior of the PL linewidth. To further study these processes, the temperature dependence of the laser emission spectra was studied. The inset of Fig. 8 shows typical laser emission spectra recorded for an injection current density of 1.1 times J_{th}. The lasing spectra exhibit a gradual narrowing with increasing temperature. This narrowing is similar for both devices, which suggests a similar temperature dependence of the homogeneous linewidth.

Hence, neither the PL nor the lasing spectra provide conclusive evidence for the TCM occurring in different temperature regions for the undoped and *p*-doped lasers. Moreover, although the broadening of the laser emission spectrum of both devices is observed at low temperatures, the linewidth of the *p*-doped laser is narrower than that of the undoped laser, whereas the PL linewidth of the *p*-doped structure is broader. This difference may indicate that the spectral broadening mechanisms are intrinsically different in PL and lasing. As suggested above, linewidth narrowing of the PL with increasing temperature results from a carrier thermal redistribution between QDs, whereas the linewidth of the laser emission spectra is determined by the homogeneous broadening of the optical gain. It should also be noted that the lasing spectra of the *p*-doped device are much narrower than those of the undoped device for temperatures above 77 K, indicating a larger homogeneous linewidth for the *p*-doped device.

B. Thermal redistribution with different injections

As discussed above, the broadening of the lasing spectra at low temperatures may result from the homogeneous broadening of the optical gain, rather than effects related to the TCM. One possible reason for this is that the contribution from the TCM is reduced as the injection current approaches threshold. To study this behavior, the thermal redistribution of carriers between the two QD subsets for different injection levels has been calculated. A thermal coupling factor K_{thermal} is introduced to describe the degree of TCM, as shown in Fig. 9. For a bimodal distribution of dots,

$$K_{\mathrm{thermal}}=\frac{n_{GS}^{2}}{n_{GS}^{1}}. \tag{16}$$

The dotted line in Fig. 9 indicates $K_{\mathrm{thermal}}=1$ and corresponds to an equal distribution of carriers within the two subsets of dots.

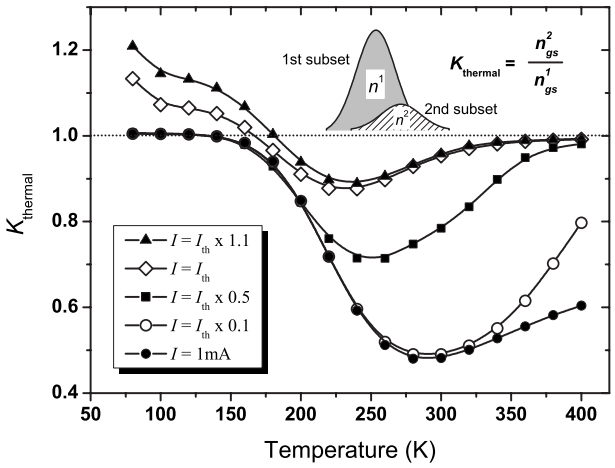

FIG. 9. The temperature dependence of the thermal coupling factor $K_{thermal}$ for the *p*-doped QD laser and different current injection levels. The inset shows the definition of $K_{thermal}$.

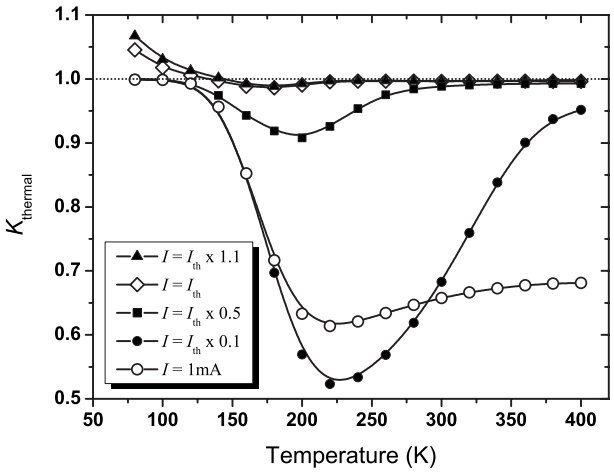

FIG. 10. The temperature dependence of the thermal coupling factor $K_{thermal}$ for the undoped QD laser and for different injection levels.

Figure 9 shows the temperature dependence of the thermal coupling factor for the *p*-doped QD laser calculated for different levels of injection current from $I=1$ mA to $I_{th} \times 1.1$. For a current of 1 mA, $K_{thermal}$ decreases from 1.0 at 100 K to a minimum value of 0.48 at 280 K; this reflects a thermal redistribution process between the two subsets of QDs. Almost half of the carriers in the second, smaller subset of dots are thermally excited into the barrier and some of these are recaptured into the first subset of larger dots. However, with increasing current, the thermal redistribution process weakens significantly, with a minimum $K_{thermal}$ of 0.9 achieved at 250 K for a current of $I_{th} \times 1.1$. This value for currents just above the threshold suggests that the TCM is less significant at and above threshold in the *p*-doped device. In Fig. 10, the thermal coupling factor for the undoped QD laser is plotted. At a current of 1 mA, $K_{thermal}$ decreases from 1.0 at 100 K to a minimum value of 0.52 at 220 K. Again, the strength of the thermal redistribution process is reduced significantly for a current of $I_{th} \times 1.1$. The reason for this decreasing strength of the thermal redistribution process as the current approaches threshold is because the faster carrier recombination rate reduces the fraction of carriers able to escape from the subset of smaller QDs before radiative recombination occurs.

In the low-temperature regime below 200 K, it can be seen that the thermal coupling factor can reach a value greater than 1.0. A value greater than 1 reflects strong carrier spectral hole burning, which occurs at low temperatures near 100 K due to blocked carrier excitations, as described in Eq. (15) by the exponential factor $1/\exp((E_{ES}-E_{GS})/kT)$ with a very small value of kT. This blocked carrier excitation may be responsible for a slower polarization dephasing rate, as well as a broader laser emission spectrum, which has been previously discussed in relation to the homogeneous broadening model.[20] The results of Figs. 9 and 10 indicate that while the TCM is an important process for injection levels below threshold, its importance is less at and above threshold.

A comparison of Figs. 9 and 10 indicates that the critical temperature of the TCM is different in the *p*-doped and undoped devices. At an injection current of 1 mA, the critical temperature is 280–300 K in the *p*-doped device and 220 K in the undoped device. These temperatures agree very well with experimental studies of a TCM delayed by ~70 K in the EL results of Refs. 32 and 33, as well as the PL data in the present work. The main reason for the delayed critical temperature predicted by the present simulations is due to a delayed electron escape process in the *p*-doped device. From Eq. (13), it is found that a slower electron escape process at a given temperature requires a smaller ES occupancy. The ES electron occupancy is lower in the *p*-doped device compared to the undoped device at injection levels far below threshold, because a faster spontaneous recombination rate occurs due to the presence of the extrinsic holes. It should be noted that this delayed critical temperature is mainly affected by the thermal escape process described in Eq. (13), whereas the delayed intradot thermal excitation in Fig. 7(a) is dominated by the thermal excitation process described in Eq. (15). However, the reason for these two kinds of delay is similar, both of which result from reduced electron occupation factors in the QD states of the *p*-doped device.

In addition to the processes included in the present simulations, an increased electron confinement has been proposed as a mechanism for a delayed TCM in *p*-type devices.[25] This arises from the Coulomb attraction by the extrinsic holes. However, it is difficult to evaluate by how much the electron confinement will be altered by the extrinsic holes, and in the present simulations, the same electron and hole confinement potentials are assumed for both devices. Including a deeper electron confinement potential in the simulation results, the TCM minimum shifts to a higher temperature, as expected. However, in the absence of an accurate knowledge of the magnitude of the increased confinement potential that results from the extrinsic holes, this modified potential has not been included in the simulations presented in this paper.

With increasing current injection, the critical temperature at which the minimum $K_{thermal}$ occurs is reduced, for example, to 220 K at threshold for the *p*-doped device. The same phenomenon can be observed in the undoped device

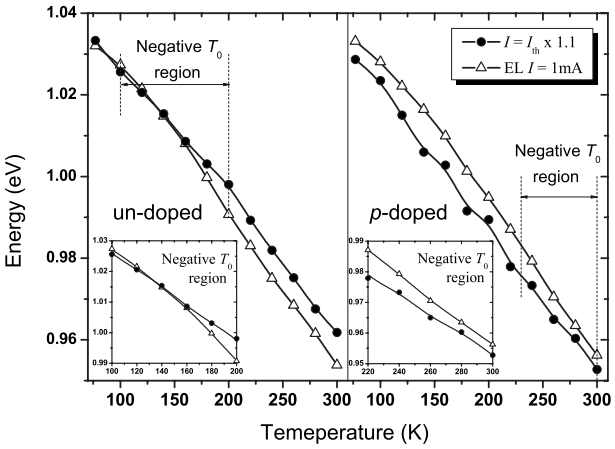

FIG. 11. The temperature dependence of the emission wavelength for two injection currents and for both the *p*-doped and undoped QD lasers.

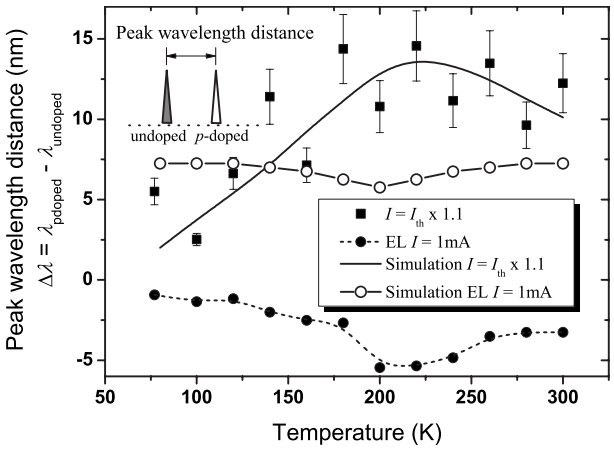

FIG. 12. Temperature dependence of the difference between the peak wavelengths of the undoped and *p*-doped QD lasers for both low-current injection and injection above threshold.

where the critical temperature changes from 220 to 160 K as the injection current increases from 1 mA to threshold. The K_{thermal} minima at threshold, predicted by the simulations plotted in Figs. 9 and 10, occur at the same temperature as the minima in J_{th} simulated by only considering the TCM (see inset of Fig. 5). It can hence be concluded that the significance of the TCM is weakened at high-injection currents and on its own appears unable to fully account for the negative T_0 observed in both *p*-doped and undoped lasers.

C. Wavelength shift

Finally, the predictions of the TCM and PCM for the temperature dependence of the emission wavelength are considered. Low-current EL spectra and lasing spectra (EL spectra above threshold) were measured for comparison with the simulations. Figure 11 shows the measured temperature dependence of the EL emission for injection currents of $I = 1$ mA and $I_{\text{th}} \times 1.1$ for both devices. The gross shift of the emission is caused by the thermal band gap shrinkage, which is not known accurately enough to reliably remove it from the experimental data. Hence, it is necessary to look for small effects against this background shift via a comparison of the emission at the two different injection currents. Relative to the EL at 1 mA, the lasing emission exhibits a blueshift below 200 K for the undoped device and above 220 K for the *p*-doped device. These are the temperature regions where the negative T_0 is observed for both devices. This behavior agrees with the predictions of the PCM as discussed above. The detailed behavior of the emission in the negative T_0 regions is shown in the insets of Fig. 11 for both devices. Relative to the low-injection current EL, the lasing emission exhibits a blueshift of 10 meV for the undoped device and 5 meV for the *p*-doped device.

Because the temperature dependence of the QD band gap is not accurately known, it is not easy to simulate the emission behavior shown in Fig. 11. However, if only the wavelength difference between the undoped and *p*-doped devices is considered, the effects of the temperature-dependent band gap can be neglected if it is assumed that this is the same for both devices. Figure 12 shows the measured temperature dependence of the emission difference between the undoped and *p*-doped devices for a range of injection currents. The peak emission is taken as the maximum of the whole spectra, which contains contributions from both subsets of dots; this is particularly significant in the low-injection spectra. The inset shows a schematic of the quantity plotted in the main part of the figure. Below 200 K, the lasing emission is dominated by the photon coupling process, which gives a blueshift in the undoped device and a redshift in the *p*-doped device. As a result, the wavelength separation between the devices increases with increasing temperature. In contrast, the low-current behavior is dominated by a thermal redistribution process, which gives a redshift for both the undoped and *p*-doped devices. However, the thermal redistribution process is delayed in the *p*-doped device by ~70 K as discussed above. This delay results in the separation between the two devices decreasing above ~170 K, and this separation does not return to its pre-170-K value until the thermal redistribution process is completed in the *p*-doped device. The results plotted in Fig. 12 reveal a very different behavior for the lasing emission and subthreshold EL below 200 K.

Figure 12 also contains the results of a simulation based on the theoretical model described above and assuming a bimodal distribution of dots. Assuming a wavelength separation of 2 nm at 80 K between the lasing spectra of the undoped and *p*-doped devices, the simulation results describe well the experimental results for above threshold injection. The simulated lasing wavelength difference increases by 11 nm between 80 and 220 K. Experimentally, the increase is 10 nm between 80 and 190 K. For low-current injection, the simulated and experimental values are 2 and 4 nm, respectively. The differences between the experimental and simulated results may result from an underestimation of the thermal-carrier redistribution between the subgroups of QDs. As in other simulations discussed above, the results presented in Fig. 12 indicate that the effect of the TCM is significant at low-injection current but that the PCM is needed to fully explain the wavelength behavior above threshold.

V. CONCLUSION

In summary, a theoretical model accounting for both thermal coupling and photon coupling processes in self-assembled QD lasers has been presented. The presence of a negative T_0 region where a spectral blueshift coexists in both undoped and *p*-doped QD lasers can be explained by a photon coupling process between the GS and the first ES in dots of different sizes. The intradot thermal excitation of electrons is delayed in a *p*-type device, a result of a reduced electron occupation of the GS. This behavior when combined with the PCM can account for the very different temperature dependence of J_{th} observed in the two types of device. Below threshold, the TCM results in a spectral linewidth narrowing and a redshift of the emission for both undoped and *p*-doped QD devices with increasing temperature. This behavior is weakened as the injection level is increased. Near and above threshold, the PCM makes an increased contribution to the behavior of the lasers.

*c.jin@sheffield.ac.uk

[1] Y. Arakawa and H. Sakaki, Appl. Phys. Lett. **40**, 939 (1982).
[2] M. Asada, Y. Miyamoto, and Y. Suematsu, IEEE J. Quantum Electron. **QE-22**, 1915 (1986).
[3] D. Leonard, M. Krishnamurthy, C. M. Reaves, S. P. Denbaars, and P. M. Petroff, Appl. Phys. Lett. **63**, 3203 (1993).
[4] N. Kirstaedter, N. N. Ledentsov, M. Grundmann, D. Bimberg, V. M. Ustinov, S. S. Ruvinov, M. V. Maximov, P. S. Kop'ev, Z. I. Alferov, U. Richter, P. Werner, U. Gosele, and J. Heydenreich, Electron. Lett. **30**, 1416 (1994).
[5] G. T. Liu, A. Stintz, H. Li, K. J. Malloy, and L. F. Lester, Electron. Lett. **35**, 1163 (1999).
[6] I. R. Sellers, H. Y. Liu, K. M. Groom, D. T. Childs, D. Robbins, T. J. Badcock, M. Hopkinson, D. J. Mowbray, and M. S. Skolnick, Electron. Lett. **40**, 1412 (2004).
[7] H. Y. Liu, D. T. Childs, T. J. Badcock, K. M. Groom, I. R. Sellers, M. Hopkinson, R. A. Hogg, D. J. Robbins, D. J. Mowbray, and M. S. Skolnick, IEEE Photonics Technol. Lett. **17**, 1139 (2005).
[8] O. B. Schekin, G. Park, D. L. Huffaker, and D. G. Deppe, Appl. Phys. Lett. **77**, 466 (2000).
[9] L. V. Asryan and R. A. Suris, Semicond. Sci. Technol. **11**, 554 (1996).
[10] A. E. Zhukov, V. M. Ustinov, A. Y. Egorov, A. R. Kovsh, A. F. Tsatsulnikov, N. N. Ledentsov, S. V. Zaitsev, N. Y. Geordeev, P. S. Kopev, and Z. I. Alferov, Jpn. J. Appl. Phys., Part 1 **36**, 4216 (1997).
[11] D. I. Lubyshev, P. P. González-Borrero, E. Marega, Jr., E. Petitprez, N. La Scala, Jr., and P. Basmaji, Appl. Phys. Lett. **68**, 205 (1996).
[12] Z. Y. Xu, Z. D. Lu, X. P. Yang, Z. L. Yuan, B. Z. Zheng, J. Z. Xu, W. K. Ge, Y. Wang, J. Wang, and L. L. Chang, Phys. Rev. B **54**, 11528 (1996).
[13] L. Brusaferri, S. Sanguinetti, E. Grilli, M. Guzzi, A. Bignazzi, F. Bogani, L. Carraresi, M. Colocci, A. Bosacchi, P. Frigeri, and S. Franchi, Appl. Phys. Lett. **69**, 3354 (1996).
[14] S. Sanguinetti, M. Henini, M. Grassi Alessi, M. Capizzi, P. Frigeri, and S. Franchi, Phys. Rev. B **60**, 8276 (1999).
[15] A. Patane, A. Polimeni, M. Henini, L. Eaves, P. C. Main, and G. Hill, J. Appl. Phys. **85**, 625 (1999).
[16] K. M. Groom, A. I. Tartakovskii, D. J. Mowbray, M. S. Skolnick, P. M. Smowton, M. Hopkinson, and G. Hill, Appl. Phys. Lett. **81**, 1 (2002).
[17] M. Grundmann and D. Bimberg, Jpn. J. Appl. Phys., Part 1 **36**, 4181 (1997).
[18] M. Grundmann, O. Stier, S. Bognar, C. Ribbat, F. Heinrichsdorff, and D. Bimberg, Phys. Status Solidi A **178**, 255 (2000).
[19] H. Huang and D. G. Deppe, IEEE J. Quantum Electron. **37**, 691 (2001).
[20] M. Sugawara, K. Mukai, Y. Nakata, H. Ishikawa, and A. Sakamoto, Phys. Rev. B **61**, 7595 (2000).
[21] M. Sugawara, K. Mukai, and Y. Nakata, Appl. Phys. Lett. **74**, 1561 (1999).
[22] O. B. Shchekin and D. G. Deppe, Appl. Phys. Lett. **80**, 3277 (2002).
[23] O. B. Shchekin, J. Ahn, and D. G. Deppe, Electron. Lett. **38**, 712 (2002).
[24] S. Fathpour, Z. Mi, P. Bhattacharya, A. R. Kovsh, S. S. Mikhrin, I. L. Krestnikov, A. V. Kozhukhov, and N. N. Ledentsov, Appl. Phys. Lett. **85**, 5164 (2004).
[25] I. P. Marko, N. F. Masse, S. J. Sweeney, A. D. Andreev, A. R. Adams, N. Hatori, and M. Sugawara, Appl. Phys. Lett. **87**, 211114 (2005).
[26] H. Y. Liu, S. L. Liew, T. Badcock, D. J. Mowbray, M. S. Skolnick, S. K. Ray, T. L. Choi, K. M. Groom, B. Stevens, F. Hasbullah, C. Y. Jin, M. Hopkinson, and R. A. Hogg, Appl. Phys. Lett. **89**, 073113 (2006).
[27] T. J. Badcock, H. Y. Liu, K. M. Groom, C. Y. Jin, M. Gutiérrez, M. Hopkinson, D. J. Mowbray, and M. S. Skolnick, Electron. Lett. **42**, 922 (2006).
[28] C. Y. Jin, T. J. Badcock, H. Y. Liu, K. M. Groom, R. J. Royce, D. J. Mowbray, and Mark Hopkinson, IEEE J. Quantum Electron. **42**, 1259 (2006).
[29] H. Y. Liu, I. R. Sellers, T. J. Badcock, D. J. Mowbray, M. S. Skolnick, K. M. Groom, M. Gutiérrez, M. Hopkinson, J. S. Ng, J. P. R. David, and R. Beanland, Appl. Phys. Lett. **85**, 704 (2004).
[30] C. Y. Jin, H. Y. Liu, T. J. Badcock, K. M. Groom, D. J. Mowbray, and M. Hopkinson, IEE Proc.: Optoelectron. **153**, 280 (2006).
[31] S. Ghosh, P. Bhattacharya, E. Stoner, J. Singh, H. Jiang, S. Nuttinck, and J. Laskar, Appl. Phys. Lett. **79**, 722 (2001).
[32] I. C. Sandall, P. M. Smowton, J. D. Thomson, T. Badcock, D. J. Mowbray, H.-Y. Liu, and M. Hopkinson, Appl. Phys. Lett. **89**, 151118 (2006).
[33] T. J. Badcock, R. J. Royce, D. J. Mowbray, M. S. Skolnick, H. Y. Liu, M. Hopkinson, K. M. Groom, and Q. Jiang, Appl. Phys. Lett. **90**, 111102 (2007).
[34] H. Y. Liu, M. Hopkinson, C. N. Harrison, M. J. Steer, R. Frith, I. R. Sellers, D. J. Mowbray, and M. S. Skolnick, J. Appl. Phys. **93**, 2931 (2003).
[35] H. Y. Liu, I. R. Sellers, M. Gutierrez, K. M. Groom, W. M.

Soong, M. Hopkinson, J. P. R. David, R. Beanland, T. J. Badcock, D. J. Mowbray, and M. S. Skolnick, J. Appl. Phys. **96**, 1988 (2004).
[36] M. Sugawara, N. Hatori, H. Ebe, M. Ishida, and Y. Arakawa, J. Appl. Phys. **97**, 043523 (2005).
[37] S. Osborne, P. Blood, P. Smowton, J. Lutti, Y. C. Xin, A. Stintz, D. Huffaker, and L. F. Lester, IEEE J. Quantum Electron. **40**, 1639 (2004).
[38] G. Park, O. B. Shchekin, and D. G. Deppe, IEEE J. Quantum Electron. **36**, 1065 (2000).
[39] D. G. Deppe, H. Huang, and O. B. Shchekin, IEEE J. Quantum Electron. **38**, 1587 (2002).
[40] D. Bimberg, N. Kirstaedter, N. N. Ledentsov, Zh. I. Alferov, P. S. Kop'ev, and V. M. Ustinov, IEEE J. Quantum Electron. **3**, 196 (1997).
[41] C. Y. Jin, Y. Z. Huang, L. J. Yu, and S. L. Deng, IEEE J. Quantum Electron. **40**, 513 (2004).
[42] T. W. Berg and J. Mørk, IEEE J. Quantum Electron. **40**, 1527 (2004).
[43] M. A. Lampert and P. Mark, *Current Injection in Solid* (Academic, New York, 1970).
[44] Y. C. Zhang, C. J. Huang, F. Q. Liu, B. Xu, J. Wu, Y. H. Chen, D. Ding, W. H. Jiang, X. L. Ye, and Z. G. Wang, J. Appl. Phys. **90**, 1973 (2001).
[45] P. Borri, W. Langbein, J. Mørk, J. M. Hvam, F. Heinrichsdorff, M.-H. Mao, and D. Bimberg, Phys. Rev. B **60**, 7784 (1999).
[46] P. Borri, W. Langbein, S. Schneider, U. Woggon, R. L. Sellin, D. Ouyang, and D. Bimberg, IEEE J. Quantum Electron. **8**, 984 (2002).